Transfer hydrogenation of nitroarenes to arylamines catalysed by an oxygen-implanted MoS$_2$ catalyst

Chaofeng Zhang [a,b], Zhixin Zhang [a], Xu Wang [c], Mingrun Li [a], Jianmin Lu [a], Rui Si [c], Feng Wang [a,*]

[a] State Key Laboratory of Catalysis, Dalian National Laboratory for Clean Energy Dalian Institute of Chemical Physics, Chinese Academy of Sciences, Dalian 116023, Liaoning, China
[b] Graduate University of Chinese Academy of Sciences, Beijing 100049, China
[c] Shanghai Synchrotron Radiation Facility, Shanghai Institute of Applied Physics, Chinese Academy of Sciences, Shanghai 201204, China

ABSTRACT

We present an efficient approach for chemoselective synthesis of various functionalized arylamines from nitroarenes over an oxygen-implanted MoS$_2$ catalyst (O-MoS$_2$). The HRTEM, XRD, XPS, Raman, EXAFS and NH$_3$-TPD characterizations show the existence of Mo^{IV}O$_x$ structure and abundant coordinative unsaturated (CUS) Mo sites in the 2D-layer structure of O-MoS$_2$. In the transfer hydrogenation of nitroarenes with hydrazine hydrate, the Mo^{IV}O$_x$ structure works as the catalytic active center. The N$_2$H$_4$ selectively decomposes to the active hydrogen species in polar electronic states (H$^{\delta-}$ and H$^{\delta+}$), which show high chemoselectivity toward the nitro reduction over C=C, C=C, and C≡N groups. The O-MoS$_2$ catalyst can be recovered in a facile manner from the reaction mixture and recycled four times without any significant loss of activity.

© 2016 Elsevier B.V. All rights reserved.

1. Introduction

Functionalized arylamines prepared from its corresponding nitroarenes are very important industrial intermediates for pharmaceuticals, functional polymers, herbicides, dyestuffs and other fine chemicals [1]. Previous studies on nitroarene reduction majorly focused on oxide-supported catalysts containing d$_6$–d$_{10}$ metals [2–16]. Besides their oxidizable nature in the air, the selectivity of the corresponding amines was not high enough when other reducible functional groups were present in the same molecules. Regarding the storage and availability, robust non-precious metal oxides have attracted attentions for nitroarene reduction, but oxide catalysts with high activity are still rarely used [17–23]. So, researches on new catalytic methods and the intrinsic mechanism should be done.

Recently, in the nitroarenes catalytic transformation, numbers of effective and selective approaches with various oxide-supported Au [24–33], Pt [34] and Ag [35] catalysts have been developed. Besides the catalytic approaches exploitation, Corma and co-workers found the cooperative effects between gold and the support played crucial roles in the selective activation of substrates [26] and hydrogenation route control [36]. Kaneda and co-workers found that the metal-oxide interfacial structure played crucial roles in the hydrogenation of nitro and alkynyl groups with active hydrogen species in polar electronic states [35,37,38]. The metal-oxide interfacial structure can dynamically stabilize the in-situ generated hydride and proton via a cooperative effect of metallic and basic sites [35].

Since most of the pure metal oxides lack the required metallic properties, the redox character of central metal plays crucial roles in the catalysis [19]. It is understandable that most pure metal oxide catalysts are inactive in nitroarenes catalytic reduction. Recently, Beller and co-workers found that Fe$_2$O$_3$ and CoO$_x$ particles surrounded by nitrogen-doped carbon layers were efficient catalysts for the selective hydrogenation [39–41] and transfer hydrogenation [42–44] of nitroarenes to anilines. The nitrogen-doped carbon layers and MN$_x$ (M = Co, Fe) species of the oxide catalysts account for the high activity.

Without doping or other modification methods, we recently found that the crystalline MoO$_2$, with inherent bifunctional metallic-basic character, was an effective catalyst for the transfer hydrogenation of nitrobenzene with N$_2$H$_4$ [23]. Density functional theory (DFT) calculations suggest that the stepwise hydrogen transfer via the prior cleavage of N—H bond than N—N bond is the key

step to create the dissociated hydride and proton species on the surface $Mo^{IV}O_x$ center. However, the MoO_2 surface can be oxidized, and the adsorbed ammonia can prevent the oxidized sites reduction with N_2H_4, which causes the catalyst deactivation. The used catalyst needs calcination regeneration in recycle using.

In this work, we prepared an oxygen-implanted MoS_2 catalyst ($O-MoS_2$) via an incomplete sulfidation and reduction method. The ammonium molybdate was used as the precursor, and some $Mo^{IV}O_x$ structure was left to $O-MoS_2$. The $O-MoS_2$ can efficiently catalyse nitroarenes reduction to the corresponding arylamines with N_2H_4 under air condition, and the used catalyst can be easily recovered and reused four times without any significant loss of activity. Different from previous MoS_2-based catalysts with MoS_2 skeleton as the active center for the nitroarenes reduction [45–50], results of this work propose that the $Mo^{IV}O_x$ structure implanted in $O-MoS_2$ works as the active center. The $O-MoS_2$ can catalyse the N_2H_4 selective decomposition to the active hydrogen species in polar electronic states ($H^{\delta-}$ and $H^{\delta+}$), which show high chemoselectivity toward the nitro reduction. The MoS_2 skeleton with metallic character around the $Mo^{IV}O_x$ structure can also catalyse N_2H_4 decomposition to create active H^*, which has the potential ability to promote the antioxidant properties of $Mo^{IV}O_x$ structure. This cooperative effect makes $O-MoS_2$ an effective and robust catalyst.

2. Experimental

2.1. Chemicals and reagents

All chemicals were of analytical grade and used as purchased without further purification.

2.2. General procedure for catalyst preparation

$O-MoS_2$ and $O-MoS_2$-Ar preparation: Typically, 3.70 g $(NH_4)_6Mo_7O_{24}\cdot4H_2O$ (3 mmol, AHM) and 6.85 g thiourea (90 mmol) were dissolved in 105 mL distilled water. The autoclave was tightly sealed in air and then placed in an oven thermally stabilized at 180 °C for 24 h, after which the autoclave was taken out and naturally cooled down to room temperature. The solid at the bottom of the reactor was centrifuged, washed with distilled water and ethanol, and dried at 60 °C under vacuum. The final solid was $O-MoS_2$. $O-MoS_2$-Ar was obtained by treating $O-MoS_2$ in Ar flow at 250 °C for 3 h.

The chemical exfoliation of commercial 2H-MoS_2 (designated as ceMoS_2) was adapted from Chou et al. [51] 700 mg of 2H-MoS_2 powder was immersed in 10 mL of *n*-butyllithium (1.6 M in hexane) and stirred for 48 h under Ar protection. After the stirring, 20 mL hexane was added into the mixture, then 0.36 mL H_2O was added dropwisely in 10 min under Ar flow. After 0.5 h, 200 mL of H_2O was added into the mixture. The mixture was sonicated at 25––30 °C for 2 h with a KUDOS ultrasonic cleaner (53 kHz) to achieve exfoliation. The ceMoS_2 nanosheets were centrifuged and washed with water and ethanol for five times over a HITACHI CR21G III centrifuge (15,000 rpm, 5 min at room temperature). The final product was obtained after vacuum drying at room temperature.

2.3. Characterization

The high-resolution transmission electron microscopy (HRTEM) was observed on a FEI Tecnai F30 electron microscope at an accelerating voltage of 300 kV. X-ray diffraction (XRD) characterizations were conducted on a Rigaku D/Max 3400 powder diffraction system with Cu $K\alpha$ radiation ($\lambda = 1.542$ Å). The X-ray photoelectron spectroscopy (XPS) measurements were carried out on a VGESCALAB MK2 spectrometer equipped with an Al $K\alpha$ X-ray

source (hυ = 1486.6 eV) at an operation voltage of 12.5 kV. The binding energy (BE) was calibrated with the C1s signal (284.6 eV) as a reference. Raman spectra was recorded on a micro-Raman spectrometer (Renishaw) equipped with a CCD detector using a He/Ne laser with a wavelength of 532 nm.

X-ray absorption fine structure (XAFS) spectra at Mo K-edge ($E_0 = 20,000$ eV) was performed at BL14W1 beam line of Shanghai Synchrotron Radiation Facility (SSRF) operated at 3.5 GeV under "top-up" mode with a constant current of 240 mA. The XAFS datas were recorded under transmission mode with ion chambers. The energy was calibrated according to the absorption edge of pure Mo foil. Athena and Artemis codes were used to extract the data and fit the profiles. For the X-ray absorption near edge structure (XANES) part, the experimental absorption coefficients as function of energies $\mu(E)$ were processed by background subtraction and normalization procedures, and reported as "normalized absorption". For the extended X-ray absorption fine structure (EXAFS) part, the Fourier transformed (FT) data in R space were analyzed by applying MoS_2 model for the Mo-S or Mo-Mo shell. The passive electron factors, S_0^2, were determined by fitting the experimental Mo foil data and fixing the Mo-Mo coordination number (CN) to be 8 + 6, then fixed for further analysis of the measured samples. The parameters describing the electronic properties (e.g., correction to the photoelectron energy origin, E_0) and local structure environment including CN, bond distance (R) and Debye Waller (D.W.) factor around the absorbing atoms were allowed to vary during the fit process.

The CUS Mo sites of MoS_2 were probed and quantitatively analyzed by temperature-programmed desorption of ammonia (NH_3-TPD). Milligrams of MoS_2 sample was loaded into a quartz tubular reactor, which was heated in a vertical electronic furnace. The desorption gas mixture was analyzed by an online mass spectrometer (THERMO^{Star} gas analysis system). The sample was initially pretreated at 100 °C under an Ar gas flow (30 mL min^{-1}) for 1 h to remove the adsorbed impurities, and then cooled down to room temperature. Then the flow gas was switched to ammonia gas (99.9%) for 30 min at room temperature, and then back to Ar gas. The reactor temperature was increased to 400 °C at a ramp rate of 10 °C min^{-1}. The m/z 17 was recorded for NH_3 and HO^* from H_2O. The pure NH_3 mass signal was the subtracted value between m/z 17 (NH_3 and HO^*) and the HO^* mass signal based on the reference mass spectrum of H_2O (m/z 18). The quantification results were calculated by referring an ammonia standard curve.

2.4. Catalytic reactions and product analyses

Nitrobenzene 0.5 mmol, solvent 2.0 mL and 50 μL *p*-xylene as an internal standard were added into a 15 mL pressure bottle with magnetic stirring. Then the hydrazine hydrate and catalyst were added into the reactor, and the reaction time was set as zero. The samples were obtained by hot filtration and analyzed by GC–MS (GC: Agilent 7890A, MS: Agilent 5975C) and GC (Agilent 7890A).

3. Results and discussion

3.1. The characterization of the O-MoS2 material

The morphology of MoS_2 materials are observed by TEM and HRTEM. Both 2H-MoS_2 (Fig. 1A and B) and ceMoS_2 (Fig. 1C and D) have a lamellar structure, and preferentially expose the basal planes with Mo and S atoms orderly arranged along (0001) crystal plane, indicating a well-crystallized phase. In contrast, the O-MoS_2 is featured with the twisted ultrathin sheets (Fig. 1E), whose atomic surface is short-range ordered but long-range disordered as illustrated in high resolution images (Fig. 1F). Except the lattice-
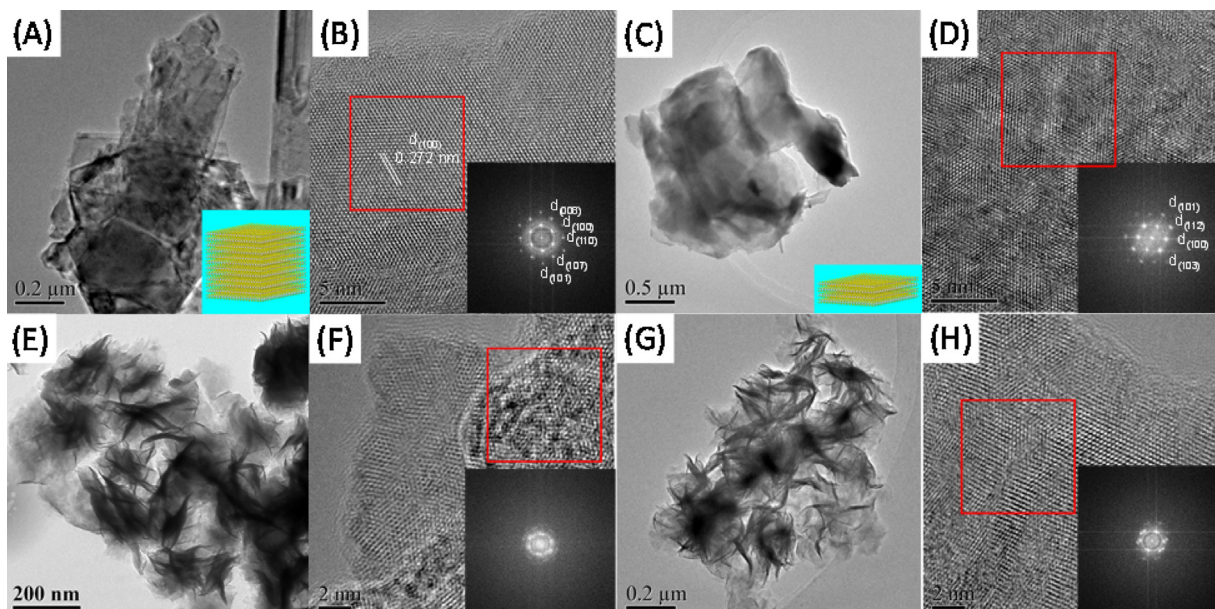
Fig. 1. The TEM and HRTEM images of 2H-MoS$_2$ (A, B), ceMoS$_2$ (C, D), O-MoS$_2$ (E, F) and O-MoS$_2$-Ar (G, H).
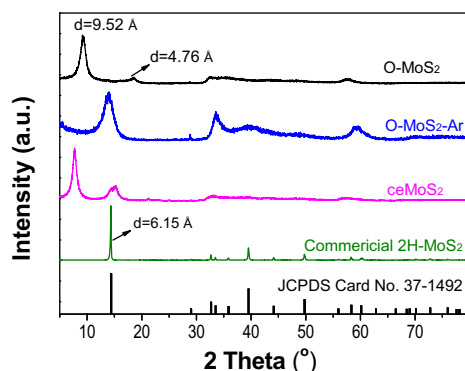

Fig. 2. The XRD patterns of the MoS$_2$ materials.

Fig. 3. XPS spectra showing the binding energies of molybdenum (A), sulfur (B), and oxygen (C) in the O-MoS$_2$.

Table 1
EXAFS fitting results of Mo-based catalysts.

Sample	Mo-S		Mo-Mo	
	R (Å)[a]	CN[b]	R (Å)[a]	CN[b]
Mo foil	–	–	2.72 ± 0.00	8
			3.14 ± 0.01	6
2H-MoS$_2$	2.40 ± 0.00	5.2 ± 0.5	3.17 ± 0.00	6.9 ± 1.3
O-MoS$_2$	2.41 ± 0.01	4.2 ± 0.5	2.77 ± 0.02	0.6 ± 0.2
O-MoS$_2$-Ar	2.40 ± 0.01	4.7 ± 0.4	3.16 ± 0.01	2.9 ± 1.1

[a] R: Distance.
[b] CN: Coordination Number.

distorted zones, a number of subnano-sized defected zones with additional edge sites are also observed on O-MoS$_2$. For the O-MoS$_2$-Ar, the thermal treatment of O-MoS$_2$ in Ar flow at 250 °C reforms the O-MoS$_2$. Consequently, its surface becomes ordered without agglomeration (Fig. 1G and H). EDX result shows that the O content was 3.7 atom% in the O-MoS$_2$ (Fig. S1) and the TPD-MS results (Fig. S2) show that there is no lattice oxygen species released from the O-MoS$_2$ as O$_2$ or SO$_2$ below 250 °C in the Ar flow.

XRD characterizations show that O-MoS$_2$ has two distinct peaks in the low-angle region with the d-spacings of 9.52 Å and 4.76 Å, respectively (Fig. 2), indicating the formation of a new lamellar structure with enlarged interlayer spacing. Thermal treatment of O-MoS$_2$ in Ar gas at 250 °C for 3 h results in the XRD pattern which resembles that of commercial 2H-MoS$_2$, signifying that the thermal treatment reforms O-MoS$_2$. It should be noted that no molybdenum oxides (MoO$_2$ or MoO$_3$) crystallites are present in O-MoS$_2$ as revealed by XRD.

As shown in XPS spectra of Mo, S and O in the O-MoS$_2$, two characteristic peaks arising from Mo 3d$_{5/2}$ and Mo 3d$_{3/2}$ orbitals are located at 229.1 and 232.2 eV (Fig. 3A), suggesting the dominance of Mo(IV) in the O-MoS$_2$ [52]. The S 2p region (Fig. 3B) exhibits primarily a single doublet with the 2p$_{3/2}$ peak at 161.7 eV, which is consistent with −2 oxidation state of sulfur [52]. Furthermore, as shown in Fig. 3C, the O 1s peak located at 530.7 eV is corresponding
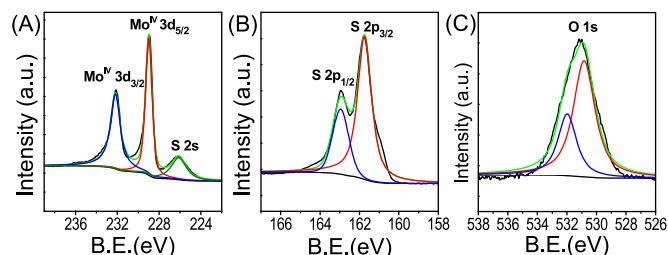
to the oxygen bonding with Mo ion [53], suggesting the existence of Mo$^{(IV)}$—O bonds, thus verifying the oxygen incorporation. The peak located at 532.0 eV can be attributed to adsorbed water. Because the molybdate precursor has Mo^{6+}, it is very reasonable that the sulfidation and reduction process is incomplete, and some Mo—O bonds are left to O-MoS$_2$. The existence various Mo—O bonds in the O-MoS$_2$ lattice structure are further revealed by the Raman spectra (Fig. S3). These characterizations show the existence of Mo^{IV}O$_x$ structure consisted of Mo^{IV}-O bonds in O-MoS$_2$.

For more information about the MoS$_2$-based materials structure, the EXAFS fitting method was adopted to check the influence of the coordination shell of the Mo atom in the O-MoS$_2$ crystal structure (Fig. S4). As shown in Table 1, the Mo-Mo structure distance (R) is 3.17 Å with a coordination number (CN) of 6.9 ± 1.3 in 2H-MoS$_2$, which are very close to the theoretical values (R$_{Mo-Mo}$ = 3.15 Å, CN$_{Mo-Mo}$ = 6) and show the commercial 2H-MoS$_2$ is in well-

Table 2
Catalyst screening and reaction condition optimization.[a]

Entry	Catalyst	Reductant	Conv.(%)[b]	Select. (%)			
				1	2	3	4
1	O-MoS$_2$	N$_2$H$_4$	>99	0	>99	0	0
2	2H-MoS$_2$	N$_2$H$_4$	41.8	5.2	60.6	8.2	26.0
3	ceMoS$_2$	N$_2$H$_4$	65.4	0	>99	0	0
4	O-MoS$_2$-Ar	N$_2$H$_4$	87.3	1.7	92.4	0.8	5.1
5	no	N$_2$H$_4$	<1.0	0	>99	0	0
6[c]	O-MoS$_2$	no	no	–	–	–	–
7[d]	Mo	N$_2$H$_4$	1.8	0	>99	0	0
8[e]	Mo	no	no	–	–	–	–
9	O-MoS$_2$	H$_2$[f]	no	–	–	–	–
10[g]	O-MoS$_2$[h]	N$_2$H$_4$	72.0	15.0	80.4	0.7	3.9
	–––[i]	N$_2$H$_4$	71.1	10.0	79.8	0.9	9.3
11[j]	O-MoS$_2$	N$_2$H$_4$	>99	0	>99	0	0
12[k]	O-MoS$_2$	N$_2$H$_4$	>99	0	>99	0	0

[a] Reaction conditions: nitrobenzene 0.5 mmol, ethanol 2.0 mL, hydrazine hydrate (80 w%) 1.5 mmol, catalyst 20 mg, Air, 50 °C for 1 h.

[b] GC Yield.

[c] No N$_2$H$_4$.

[d] Mo powders (2 μm) 12 mg.

[e] Mo powders 100 mg, no N$_2$H$_4$.

[f] H$_2$ 0.4 MPa.

[g] Hot filtration tests.

[h] 25 min.

[i] The filtrate reacted for another 25 min.

[j] The reaction scale was enlarged to the 30 times with 1.85 g PhNO$_2$.

[k] The O-MoS$_2$ reused for the fifth time.

crystallized phase. However, when 3.7 atom% oxygen (Fig. S1) is implanted into the MoS$_2$ structure via a hydrothermal synthesis method, the distance of Mo-Mo structure reduces to 2.77 Å from 3.15 Å, the CN of Mo-Mo in O-MoS$_2$ changes more obviously from 6.9 ± 1.3 to 0.6 ± 0.2, which indicates the Mo-Mo structure on the second shell almost disappears and O-MoS$_2$ has a prominent disorder degree. When the O-MoS$_2$ is treated in the Ar at 250 °C, the Mo-Mo distance in the O-MoS$_2$-Ar returns to 3.16 ± 0.01 Å, which indicates the thermal treatment reforms the lattice structure and increases the layer structure crystallinity. While the CN of Mo-Mo in O-MoS$_2$-Ar is 2.9 ± 1.1, which also shows the existence of a disordered structure. For the Mo-S structure in the MoS$_2$-based materials, Mo-S distance is almost in conformity to the theoretical value (Mo-S bond, 2.41 Å) and the CN of Mo-S structure in all materials is between 4.2 and 5.2 with a narrower range than the one of Mo-Mo structure. These results show the interaction between Mo and S in this material is strong and stable. Taking into account the facts that the oxygen content in the O-MoS$_2$ is almost ~3 atom%, the CN is 4.2 ± 0.5 for the Mo-S structure and 0.6 ± 0.2 for the Mo-Mo structure in O-MoS$_2$, O-MoS$_2$ should contain more CUS Mo sites than 2H-MoS$_2$ or O-MoS$_2$-Ar.

3.2. The performance of the O-MoS$_2$ in the nitrobenzene reduction

Our initial efforts focused on the nitrobenzene reduction at 50 °C, O-MoS$_2$ gave 99% aniline yield in 1 h (Table 2, Entry 1). Besides the O-MoS$_2$, we also employed different MoS$_2$-based material as the reference catalysts. As shown in Table 2, commercial 2H-MoS$_2$ offered a 41.8% conversion (Entry 2), ceMoS$_2$ (Entry 3) obtained by chemical exfoliation of commercial 2H-MoS$_2$ gave a 65.4% conversion. The O-MoS$_2$ treated in the Ar flow at 250 °C (O-MoS$_2$-Ar) offered a 87.3% conversion (Entry 4). No obvious reaction was observed without catalyst or without N$_2$H$_4$ (Entries 5 and 6). When Mo metal was used as a catalyst (Entry 7) or as a reductant (Entry
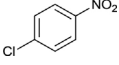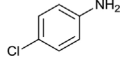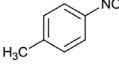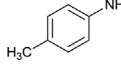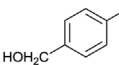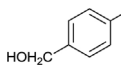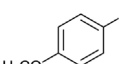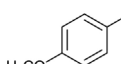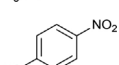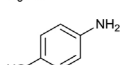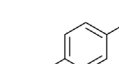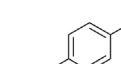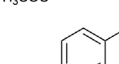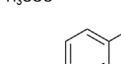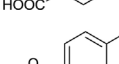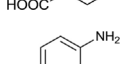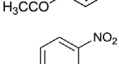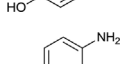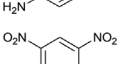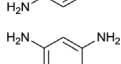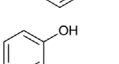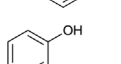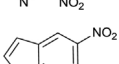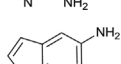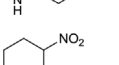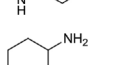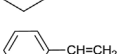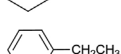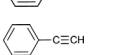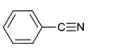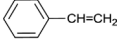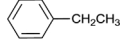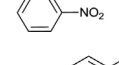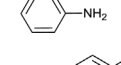
8), no obvious reaction was observed, suggesting a non-redox route [54]. Taking into account the fact that hydrazine would decompose to H$_2$ [55–58], employing H$_2$ gas in replace of N$_2$H$_4$ (Entry 9) to test whether H$_2$ was hydrogen donor gave no product, indicating O-MoS$_2$ had no ability of activating molecule hydrogen under this condition. This suggests the active hydrogen species (H*) is in-situ generated during the N$_2$H$_4$ decomposition on the surface of the O-MoS$_2$, nitroarenes reduction occurred via a transfer hydrogenation route.

Hot filtration tests showed the reaction was a heterogeneous reaction (Table 2, Entry 10). ICP analysis showed no obvious leaching of the catalyst. When the reaction scale was enlarged to 30 times with 1.85 g PhNO$_2$, >99% aniline GC yield was obtained (Table 2, Entry 11). The spent catalyst was filtered out, washed with ethanol, dried under vacuum, and then used in a new reaction. It can be reused for four cycles without any significant loss in activity (Table 2, Entry 12), which showed the stability of O-MoS$_2$ in liquid phase reactions (Fig. S5).

3.3. The substrate scope of the O-MoS$_2$ catalyst

With the excellent catalyst in hand, the substrate scope was evaluated (Table 3). 4-Chloro-aniline was synthesized in 99% GC yield and 87% isolated yield. No dehalogenation occurred (Entry 1). The substituents like −CH$_3$, −CH$_2$OH, −OCH$_3$, −OH, −COCH$_3$ and −COOH were all unaffected and well-tolerated (Entries 2–7), the products were the corresponding arylamines, respectively. The ester group of 4-nitrophenyl acetate could react with N$_2$H$_4$, its product was 4-nitrophenol (Entry 8). The nitroaniline reduction gave the 99% yield phenyl diamine in the presence of 3 equivalent hydrazine at 50 °C in 1.5 h (Entry 9). And the multiamino aromatic compounds could also be efficiently and selectively produced in the chemoselective reduction of corresponding nitroarenes (Entry 10). Notably, the O-MoS$_2$ catalyst could promote the heterocyclic nitroaromatics reduction without being deactivated by N atom

Table 3
The reduction reactions scope of the developed O-MoS$_2$ catalyst.[a]

Entry	Substrate	t (h)	N$_2$H$_4$ (equiv.)	Main Product	Conv./Select. (Yield) [%]
1	Cl–C$_6$H$_4$–NO$_2$	1	2	Cl–C$_6$H$_4$–NH$_2$	>99/>99(87.0)
2	H$_3$C–C$_6$H$_4$–NO$_2$	1	2	H$_3$C–C$_6$H$_4$–NH$_2$	>99/>99(82.3)
3	HOH$_2$C–C$_6$H$_4$–NO$_2$	1	2	HOH$_2$C–C$_6$H$_4$–NH$_2$	>99/99
4	H$_3$CO–C$_6$H$_4$–NO$_2$	1.5	3	H$_3$CO–C$_6$H$_4$–NH$_2$	>99/>99
5	HO–C$_6$H$_4$–NO$_2$	1	2	HO–C$_6$H$_4$–NH$_2$	>99/>99(93.6)
6	H$_3$COC–C$_6$H$_4$–NO$_2$	1	2	H$_3$COC–C$_6$H$_4$–NH$_2$	>99/97.8
7	HOOC–C$_6$H$_4$–NO$_2$	1	2	HOOC–C$_6$H$_4$–NH$_2$	>99/98.2
8	H$_3$CC(O)O–C$_6$H$_4$–NO$_2$	1	2	HO–C$_6$H$_4$–NH$_2$	>99/98.2
9	H$_2$N–C$_6$H$_4$–NO$_2$	1.5	3	H$_2$N–C$_6$H$_4$–NH$_2$	>99/>99
10 [b]	O$_2$N–C$_6$H$_4$–NO$_2$	1.5	3	H$_2$N–C$_6$H$_4$–NH$_2$	>99/>99
11	3-hydroxy-2-nitropyridine	1.5	3	2-amino-3-hydroxypyridine	>99/99
12	5-nitroindole	1.5	3	5-aminoindole	>99/>99
13 [b]	nitrocyclohexane	4	6	cyclohexanamine	99/75.6[c]
14	C$_6$H$_5$–CH=CH$_2$	1	2	C$_6$H$_5$–CH$_2$CH$_3$	0.3/>99
15	C$_6$H$_5$–C≡CH	1	2	–	0/–
16	C$_6$H$_5$–C≡N	1	2	–	0/–
17 [d]	C$_6$H$_5$–CH=CH$_2$ / C$_6$H$_5$–NO$_2$	1	2	C$_6$H$_5$–CH$_2$CH$_3$ / C$_6$H$_5$–NH$_2$	<1.0/>99 >99/>99
18	H$_2$C=HC–C$_6$H$_4$–NO$_2$	1	2	H$_2$C=HC–C$_6$H$_4$–NH$_2$	>99/>99

[a] Reaction condition: Substrate 0.5 mmol, ethanol 2.0 mL, O-MoS$_2$ 20 mg, Air, 50 °C.
[b] 0.25 mmol.
[c] Cyclohexanone oxime 24.4%.
[d] 0.5 mmol PhNO$_2$ and 0.5 mmol styrene.

(Entries 11–12). Besides the aromatic nitroarenes, the O-MoS$_2$ could also promote the nitrocyclohexane reduction (Entry 13).

However, O-MoS$_2$ had low activity towards catalysing the reduction of olefin, alkyne and nitrile compounds with hydrazine at 50 °C (Entries 14–16). The feature was advantageous because it could achieve the selective reduction of nitro-group in the presence of other reducible functionalities. For example, in the 1:1 molar ratio of nitrobenzene and styrene mixture, >99% aniline was obtained and ethylbenzene was only at the detectable level (<1%)

(Entry 17). When the 4-nitrostyrene was used as the substrate, 4-aminostyrene was the main product with a >99% GC yield (Entry 18).

3.4. The main reaction route of nitrobenzene reduction

Having demonstrated the utility of this method, we then focused on our interests in answering a question why O-MoS$_2$ is an efficient and robust catalyst in the chemoselective synthesis of arylamines
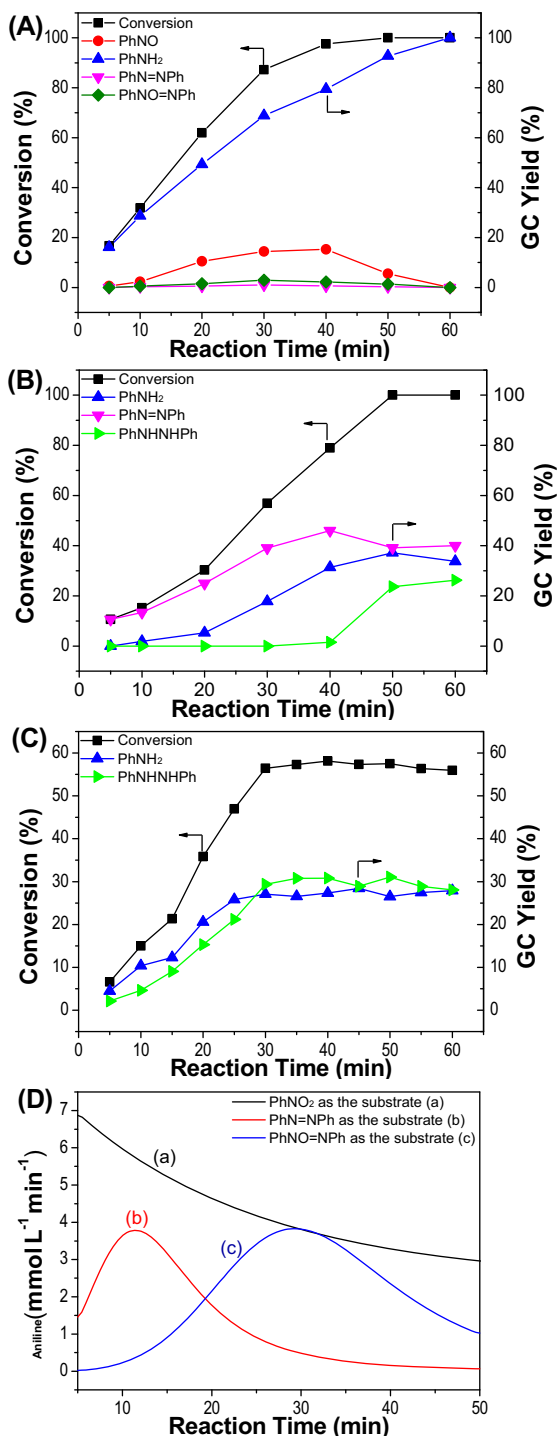
Fig. 4. The conversion-time curves of nitrobenzene (A), azoxybenzene (B), azobenzene (C) and their aniline generation rate (D). Reaction conditions: substrate n(N) = 0.5 mmol, N_2H_4 1.5 mmol, ethanol 2.0 mL, O-MoS$_2$ 20 mg, 50 °C.

from corresponding nitroarenes. For the nitroarenes reduction to arylamines, Haber proposed the reaction network [59], and there were two main routes to get the final products (Scheme S1): the direct route and the condensation route with N—N bonds formation and cleavage. In this work, besides the nitrobenzene, we also used azoxybenzene and azobenzene as the substrate to check the reaction route.

As shown in Fig. 4A, in the nitrobenzene reduction, besides the main product aniline, nitrosobenzene, azoxybenzene and azobenzene were detected. After the reaction, the only product was

the aniline. In this process, the aniline generation rate kept at 3.5–7.0 mmol L^{-1} min^{-1} (Fig. 4D). In the azoxybenzene reduction (Fig. 4B), the azoxybenzene was firstly reduced to the azobenzene, and the aniline generation rate reached ~4.0 mmol L^{-1} min^{-1} at 30 min (Fig. 4D). In the azobenzene reduction (Fig. 4C), the products were 1,2-diphenylhydrazine and aniline, before the 25 min, the aniline generation rate kept at 1.5–3 mmol L^{-1} min^{-1} (Fig. 4D). Then, the aniline generation rate decreased significantly and the azobenzene conversion reached 53.8% at 30 min and did not obviously increase in the following 30 min.

Taking into account the different aniline generation rates from nitrobenzene, azoxybenzene and azobenzene (Fig. 4D), in the nitrobenzene reduction with N_2H_4 over the O-MoS$_2$, the direct route was the main route. And, small amount of by-product generated from condensation route could also be reduced to aniline over the O-MoS$_2$. In addition, when the PhNO was used as the substrate, its conversion was 94.0% in 10 min under the same condition showed in the caption of Fig. 4, and the 79.3% selectivity to PhNH$_2$ indicated the average generation rate of aniline was 18.6 mmol L^{-1} min^{-1}. Taking into account the reduction rate of PhNO$_2$ to PhNH$_2$ (5.9–6.9 mmol L^{-1} min^{-1}), the PhNO → PhNH$_2$ should occur faster than the PhNO$_2$ → PhNO under a condition without competitive adsorption between PhNO$_2$ and PhNO on the catalyst (Scheme S2). Based on the generation rates of aniline from various substrate, PhNO$_2$ → PhNO was the rate determining step in the nitrobenzene reduction catalysed with the O-MoS$_2$.
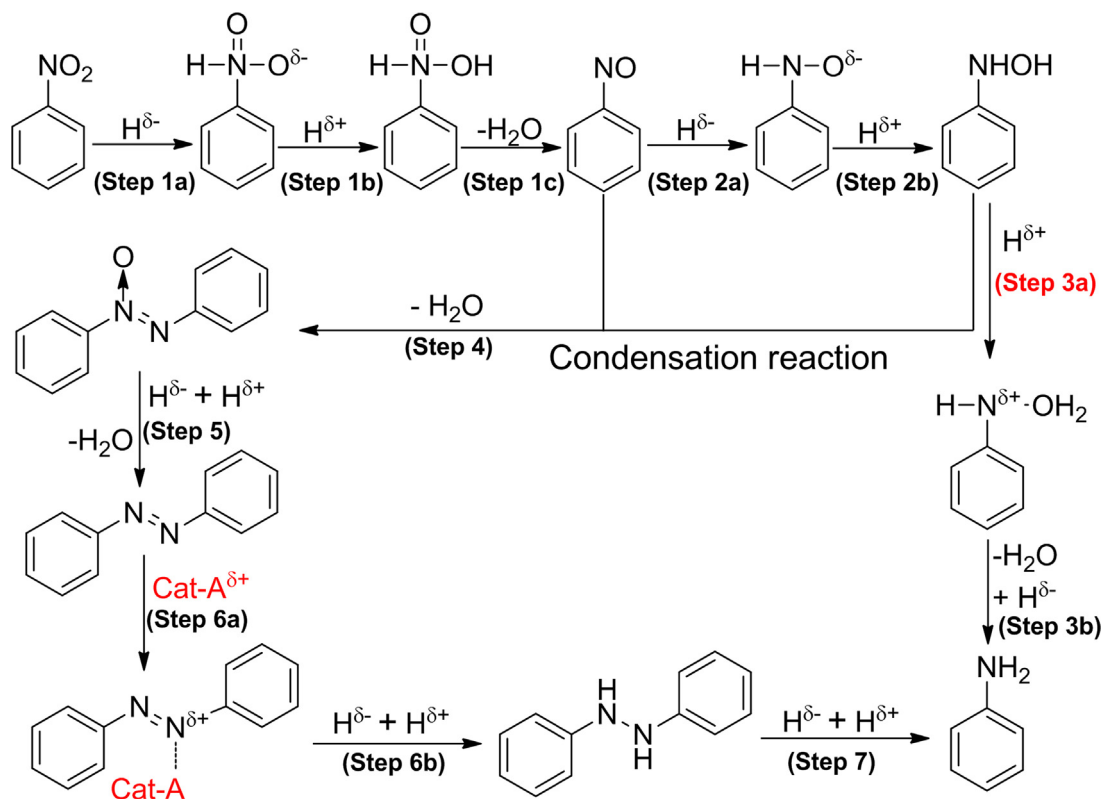
3.5. The electronic state of active hydrogen species

For most of hydrogenation reactions with substrates containing polar bonds, the heterolysis of H$_2$ molecule or other hydrogen donors to generate and stabilize hydride and proton is a premise, which often occurs over catalysts with metallic site and acid or basic sites [35,37,60,61]. As we discussed before, the nitrobenzene reduction over the O-MoS$_2$ with N_2H_4 is a transfer hydrogenation process. For the electronic state of active hydrogen species (H*) generated from N_2H_4, they can be in polar (hydride and proton, H$^{\delta-}$ and H$^{\delta+}$) or nonpolar (radical, H$^{\delta0}$) state.

If the H* exists in a nonpolar state, H$^{\delta0}$ may escape from the reaction system as H$_2$ gas. However, H$_2$ gas was not detected (Fig. S6A) and it was not an effective hydrogen donor (Table 2, Entry 9). Further experiment, adding 2,6-di-*tert*-butyl-4-methylphenol (BHT, 0.2 mmol) as the radical scavenger had no effect on catalytic result, indicated a non-radical reaction path. Considering the fact that only Mo, S and O species exist on the O-MoS$_2$ surface, if the H* combined with the O-MoS$_2$ surface, the polar electronic state might be in the lower energy state. Previous researches also showed the existence of Mo–H (H$^{\delta-}$) intermediate in transfer hydrogenation of nitroarenes with Mo-cluster or MoO$_2$ catalysts [23,47].

A linear relationship between log(k$_X$/k$_H$) and Brown–Okamoto constant σ (Fig. 5) was established for the reduction of substituted nitroarenes (X = *p*-Cl, *p*-H, *p*-CH$_3$, *p*-OCH$_3$ and *p*-NH$_2$). The Hammett parameter ρ is 0.68, suggesting that the reaction is substituent-sensitive and an anion intermediates is involved. As showed in Fig. 5, we proposed that the negative H* species (hydride, Mo–H$^{\delta-}$) participated in the slow reaction step PhNO$_2$ → PhNO. The H$^{\delta-}$ attacked the N$^{\delta+}$ atom in the —N=O bond and generated an anion intermediate [61]. The anion intermediate reacted with another H$^{\delta+}$ species and released a H$_2$O to PhNO.

As discussed above, both H$^{\delta-}$ and H$^{\delta+}$ were necessary for the reduction of the N—O or N=O bond. The base or basic sites on the catalyst could promote the heterolysis of the N—H bond in the N_2H_4 to generated active hydrogen species [58,62], but the extra base (OH$^-$) adding would increase the system pH and affect the H$^{\delta+}$ concentration. As shown in proposed nitrobenzene reduction network with active hydrogen species in polar electronic states (Scheme 1),

Scheme 1. The proposed nitrobenzene reduction network with active hydrogen speciesies in polar electronic state. Cat-A stands for the acid sites on the O-MoS$_2$ catalyst.
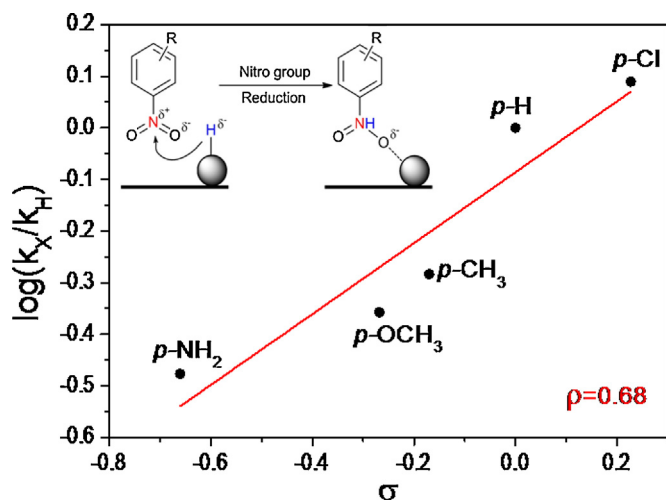

Fig. 5. Hammett plot for the nitroarenes reduction catalysed by O-MoS$_2$ with N$_2$H$_4$. The inset is the proposed way for the reduction of the N=O bond by H$^{\delta-}$ species.

Fig. 6. The effect of the NaOH on the products distribution. Reaction condition: nitrobenzene 0.5 mmol, ethanol 2.0 mL, hydrazine hydrate (80 w%) 1.5 mmol, catalyst 20 mg, Air, 50 °C, 1 h.

the low H$^{\delta+}$ concentration would inhibit the PhNHOH from further reduction to aniline (Step 3a and b), PhNHOH would tend to react with PhNO to azoxybenzene [59]. Azoxybenzene was then reduced to azobenzene, which had a neutral N=N bond and was hard reduced with polar H* directly [63]. And, in this step, adding OH$^-$ could not only change the H$^{\delta+}$ concentration but also affect the performance of acid sites to activate the N=N bond in polar state (step 6a), azobenzene further reduction would be inhibited. From this perspective, the H$^{\delta+}$ concentration change can affect the products distribution, and low H$^{\delta+}$ concentration is in favor of the generation of azobenzene. This should be the part reasons

that azobenzene synthesis from nitrobenzene usually needs base additive or the catalysts with basic support [28,33,64–66].

For further supporting the conclusion that H* should exist in polar electronic states as H$^{\delta-}$ and H$^{\delta+}$, an inhibition experiment with extra base (NaOH) was carried out (Fig. 6). When OH$^-$ (NaOH) was added to the system, the ratio of aniline as the direct-route product decreased, and the ratio of condensation route product increased. When 3.0 mmol NaOH was added, almost 50% yield of azoxybenzene and azobenzene was obtained without dynamics optimization. This result further confirmed the suggestion that the H* should be in polar electronic states as H$^{\delta-}$ and H$^{\delta+}$.

3.6. The reaction mechanism of nitroarenes reduction

In order to further study the reaction mechanism, we analyzed gas product with mass spectrometry. As shown in Fig.
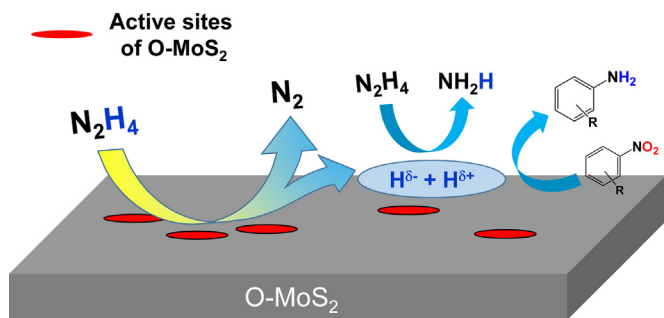
Scheme 2. Plausible reaction mechanism of nitroarenes reduction.

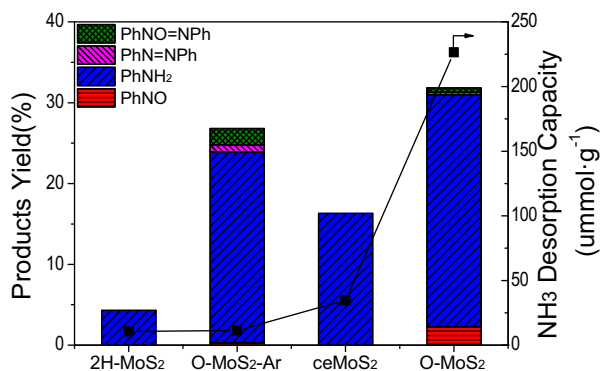**Fig. 7.** The effect of the CUS Mo site on the nitrobenzene with N_2H_4 over the MoS_2-based catalyst. Reaction condition: nitrobenzene 0.5 mmol, ethanol 2.0 mL, hydrazine hydrate (80 w%) 1.5 mmol, catalyst 20 mg, Air, 50 °C for 10 min. CUS Mo sites was estimated with the NH_3-TPD results.

S6, N_2 ($m/z = 28$) was detected in the gas phase with or without nitrobenzene. No H_2 ($m/z = 2$) was detected in both cases. With the reaction proceeding, $m/z = 17$ (NH_3 and HO^*) signal line was higher than the $m/z = 18$ (H_2O) one, which showed the generation of NH_3 in the gas phase. Generally speaking, the typical reaction route for hydrazine decomposition was $3N_2H_4 \rightarrow 4(1-x)NH_3 + (1+2x)N_2 + 6xH_2$ [58,67]. So, hydrazine decomposition over O-MoS_2 occurred according to the equation of $3N_2H_4 \rightarrow N_2 + 4NH_3$. Two N_2H_4 were reduced to four NH_3 with four active H^* [68,69], and the other N_2H_4 molecular should transform into one N_2 molecular and four H^* [23].

Based on the above discussion, the H^* could exist as $H^{\delta-}$ and $H^{\delta+}$, and nitrobenzene reduction with N_2H_4 occurred via a transfer hydrogenation route. The reaction process might be that (Scheme 2): the active H^* in polar electronic states ($H^{\delta-}$ and $H^{\delta+}$) were generated from N_2H_4 via N—H bond activation on the O-MoS_2, then $H^{\delta-}$ and $H^{\delta+}$ species reacted with nitro to amine or with hydrazine to NH_3, and the catalytic active sites restored to the original state.

3.7. The catalytic active structure of the O-MoS_2

As a typical 2D-layer material, the coordinative unsaturated (CUS) edge Mo sites in the MoS_2 structure usually played crucial roles in the catalysis process [47,52,70–76]. We used the NH_3-TPD characterization to estimate the amount of CUS Mo sites on the Mo based catalyst. As shown in Fig. 7, the NH_3 desorption capacity of 2H-MoS_2 was only 10.7 μmol g^{-1}, chemical exfoliation method made ceMoS_2 a higher one and the value reached 34.8 μmol g^{-1}. In comparison, the O-MoS_2 NH_3 desorption capacity was 7 times (226.4 μmol g^{-1}) of ceMoS_2. After treatment in Ar at 250 °C, the value was remarkably decreased to 11.2 μmol g^{-1} for the O-MoS_2-Ar. In the nitrobenzene reduction over various cat-

alysts, the conversions over 2H-MoS_2, ceMoS_2 and O-MoS_2 were 4.3%, 16.3% and 32.0%, respectively. The relationship between conversion and NH_3 desorption capacity or the CUS Mo site was not a positive correlation (Fig. 7). These results showed the promotion of CUS Mo sites in nitrobenzene conversion was limited.

The nitrobenzene conversion over O-MoS_2-Ar with few CUS Mo sites reached 27.0% at 10 min (Fig. 7), which was as good as O-MoS_2 (31.8%) with abundant CUS Mo sites and much better than the 2H-MoS_2 (4.3%) with approximate amount CUS Mo sites. Given the fact that there was about 3.7 atom% O in the O-MoS_2-Ar, the difference between the conversions of 2H-MoS_2 and O-MoS_2-Ar indicated that $Mo^{IV}O_x$ structure connecting to the MoS_2 skeleton in the O-MoS_2 or O-MoS_2-Ar structure obviously promoted the reaction.

As we had reported [23], crystalline MoO_2 shows high chemoselectivity toward the nitro reduction with N_2H_4, >99% aniline yield was obtained in 30 min at 30 °C. Under the same condition, the nitrobenzene conversion over O-MoS_2 was just 17% (Fig. S7). However, the MoO_2 catalyst deactivated in the reuse experiment (Fig. S8), and the active MoO_2 surface could be partly oxidized to the worse MoO_3 (Fig. S9) phase and NH_3 generated in this reaction adsorbed on this generated MoO_3, which prevents the reaction of MoO_3 and N_2H_4 to produce the active MoO_2 (Fig. S10). However, O-MoS_2 could be reused four times without any loss in its catalytic performance and did not need regeneration operations (Fig. S5). The MoS_2 skeleton around the $Mo^{IV}O_x$ structure should have a promoting effect on the stability of the O-MoS_2.

As shown in Fig. 7, the 2H-MoS_2 or ceMoS_2 could activate N_2H_4 to the active H^* in the nitrobenzene reduction, which indicated that the MoS_2 skeleton around the $Mo^{IV}O_x$ structure should have the potential ability to achieve the oxidized Mo center reduction with the generated active H^*. In addition, the heteroatom (S^{2-}) around the $Mo^{IV}O_x$ structure could improve metal property of the active sites [77,78], which was favorable in $H^{\delta-}$ species stabilization. Based on these discussions, the cooperative effect between the active $Mo^{IV}O_x$ structure and connecting MoS_2 skeleton made O-MoS_2 an efficient and robust catalyst, which efficiently catalysed chemoselective synthesis of arylamines from corresponding nitroarenes with N_2H_4.

4. Conclusions

In summary, we present an efficient approach for chemoselective synthesis of various functionalized arylamines from corresponding nitroarenes by an oxygen-implanted MoS_2 catalyst. The robust O-MoS_2 catalyst can be easily separated and reused four times without any loss in its catalytic performance under the air condition, which is attributed to the cooperative effect between the active MoO_x structure and its surrounding MoS_2 skeleton. Furthermore, in this transfer hydrogenation reaction, the active hydrogen species in polar electronic states as $H^{\delta-}$ and $H^{\delta+}$ are generated by N—H bond activation of N_2H_4, which is beneficial for nitroarenes reduction. We believe that our findings will broaden the application of MoS_2 and MoO_x catalysts in the mild liquid-phase reactions.

Appendix A. Supplementary data

Supplementary data associated with this article can be found, in the online version, at http://dx.doi.org/10.1016/j.apcata.2016.07.008.

References

[1] R.S. Downing, P.J. Kunkeler, H. vanBekkum, Catal. Today 37 (1997) 121–136.
[2] W.J. Liu, K. Tian, H. Jiang, Green Chem. 17 (2015) 821–826.
[3] F. Li, R. Ma, B. Cao, J. Liang, Q. Ren, H. Song, Appl. Catal. A: Gen. 514 (2016) 248–252.
[4] W. Xiong, K.-J. Wang, X.-W. Liu, F. Hao, H.-Y. Xiao, P.-L. Liu, H.-A. Luo, Appl. Catal. A: Gen. 514 (2016) 126–134.
[5] J. Li, X.Y. Shi, Y.Y. Bi, J.F. Wei, Z.G. Chen, ACS Catal. 1 (2011) 657–664.
[6] Y. Jang, S. Kim, S.W. Jun, B.H. Kim, S. Hwang, I.K. Song, B.M. Kim, T. Hyeon, Chem. Commun. 47 (2011) 3601–3603.
[7] M. Pietrowski, Green Chem. 13 (2011) 1633–1635.
[8] A.B. Dongil, L. Pastor-Pérez, J.L.G. Fierro, N. Escalona, A. Sepúlveda-Escribano, Appl. Catal. A: Gen. 513 (2016) 89–97.
[9] W. Jiang, B. Xu, Z. Xiang, X. Liu, F. Liu, Appl. Catal. A: Gen. 520 (2016) 65–72.
[10] Z.Y. Sun, Y.F. Zhao, Y. Xie, R.T. Tao, H.Y. Zhang, C.L. Huang, Z.M. Liu, Green Chem. 12 (2010) 1007–1011.
[11] W.Y. Wang, D.S. Wang, X.W. Liu, Q. Peng, Y.D. Li, Chem. Commun. 49 (2013) 2903–2905.
[12] G.-Y. Fan, L. Zhang, H.-Y. Fu, M.-L. Yuan, R.-X. Li, H. Chen, X.-J. Li, Catal. Commun. 11 (2010) 451–455.
[13] K. Layek, M.L. Kantam, M. Shirai, D. Nishio-Hamane, T. Sasaki, H. Maheswaran, Green Chem. 14 (2012) 3164–3174.
[14] X. Wang, Y. Hao, M.A. Keane, Appl. Catal. A: Gen. 510 (2016) 171–179.
[15] X. Yin, D. He, P. Jiang, G. Zhou, H. Chen, Y. Deng, Appl. Catal. A: Gen. 509 (2016) 38–44.
[16] K.H.P. Reddy, R. Rahul, S.S.V. Reddy, B.D. Raju, K.S.R. Rao, Catal. Commun. 10 (2009) 879–883.
[17] A. Maltha, S.C. Vanwermeskerken, B. Brunet, V. Ponec, J. Mol. Catal. 93 (1994) 305–316.
[18] Q.X. Shi, R.W. Lu, K. Jin, Z.X. Zhang, D.F. Zhao, Green Chem. 8 (2006) 868–870.
[19] S. Kim, E. Kim, B.M. Kim, Chem. Asian J. 6 (2011) 1921–1925.
[20] D. Cantillo, M. Baghbanzadeh, C.O. Kappe, Angew. Chem. Int. Ed. 51 (2012) 10190–10193.
[21] D. Cantillo, M.M. Moghaddam, C.O. Kappe, J. Org. Chem. 78 (2013) 4530–4542.
[22] H.Z. Zhu, Y.M. Lu, F.J. Fan, S.H. Yu, Nanoscale 5 (2013) 7219–7223.
[23] C. Zhang, J. Lu, M. Li, Y. Wang, Z. Zhang, H. Chen, F. Wang, Green Chem. 18 (2016) 2435–2442.
[24] A. Corma, P. Serna, Science 313 (2006) 324–332.
[25] A. Corma, P. Serna, H. Garcia, J. Am. Chem. Soc. 129 (2007) 6358–6359.
[26] M. Boronat, P. Concepcion, A. Corma, S. Gonzalez, F. Illas, P. Serna, J. Am. Chem. Soc. 129 (2007) 16230–16237.
[27] A. Grirrane, A. Corma, H. Garcia, Science 322 (2008) 1661–1664.
[28] D. Combita, P. Concepcion, A. Corma, J. Catal. 311 (2014) 339–349.
[29] A. Corma, P. Serna, Nat. Protoc. 1 (2006) 2590–2595.
[30] X. Liu, L. He, Y.M. Liu, Y. Cao, Acc. Chem. Res. 47 (2014) 793–804.
[31] L. He, L.C. Wang, H. Sun, J. Ni, Y. Cao, H.Y. He, K.N. Ean, Angew. Chem. Int. Ed. 48 (2009) 9538–9541.
[32] F.Z. Su, L. He, J. Ni, Y. Cao, H.Y. He, K.N. Fan, Chem. Commun. (2008) 3531–3533.
[33] X. Liu, H.Q. Li, S. Ye, Y.M. Liu, H.Y. He, Y. Cao, Angew. Chem. Int. Ed. 53 (2014) 7624–7628.
[34] H. Wei, X. Liu, A. Wang, L. Zhang, B. Qiao, X. Yang, Y. Huang, S. Miao, J. Liu, T. Zhang, Nat. Commun. 5 (2014) 5634–5642.
[35] T. Mitsudome, Y. Mikami, M. Matoba, T. Mizugaki, K. Jitsukawa, K. Kaneda, Angew. Chem. Int. Ed. 51 (2012) 136–139.
[36] A. Corma, P. Concepcion, P. Serna, Angew. Chem. Int. Ed. 46 (2007) 7266–7269.
[37] A. Noujima, T. Mitsudome, T. Mizugaki, K. Jitsukawa, K. Kaneda, Angew. Chem. Int. Ed. 50 (2011) 2986–2989.
[38] T. Mitsudome, M. Yamamoto, Z. Maeno, T. Mizugaki, K. Jitsukawa, K. Kaneda, J. Am. Chem. Soc. 137 (2015) 13452–13455.
[39] R.V. Jagadeesh, A.-E. Surkus, H. Junge, M.-M. Pohl, J. Radnik, J. Rabeah, H. Huan, V. Schuenemann, A. Brueckner, M. Beller, Science 342 (2013) 1073–1076.
[40] F.A. Westerhaus, R.V. Jagadeesh, G. Wienhofer, M.M. Pohl, J. Radnik, A.E. Surkus, J. Rabeah, K. Junge, H. Junge, M. Nielsen, A. Bruckner, M. Beller, Nat. Chem. 5 (2013) 537–543.
[41] D. Formenti, C. Topf, K. Junge, F. Ragaini, M. Beller, Catal. Sci. Technol. 6 (2016) 4473–4477.
[42] R.V. Jagadeesh, G. Wienhofer, F.A. Westerhaus, A.E. Surkus, M.M. Pohl, H. Junge, K. Junge, M. Beller, Chem. Commun. 47 (2011) 10972–10974.
[43] F.A. Westerhaus, I. Sorribes, G. Wienhofer, K. Junge, M. Beller, Synlett 26 (2015) 313–317.
[44] R.V. Jagadeesh, K. Natte, H. Junge, M. Beller, ACS Catal. 5 (2015) 1526–1529.
[45] S.K. Srivastava, B.N. Avasthi, J. Mater. Sci. 28 (1993) 5032–5035.
[46] D.Y. Sun, B.Z. Lin, B.H. Xu, L.W. He, C. Ding, Y.L. Chen, J. Porous Mater. 15 (2008) 245–251.
[47] I. Sorribes, G. Wienhofer, C. Vicent, K. Junge, R. Llusar, M. Beller, Angew. Chem. Int. Ed. 51 (2012) 7794–7798.
[48] L. Huang, P.F. Luo, P. Xiong, R.Z. Chen, Y. Wang, W.H. Xing, J. Huang, Chin. J. Chem. 31 (2013) 987–991.
[49] S. Kamiguchi, K. Arai, K. Okumura, H. Iida, S. Nagashima, T. Chihara, Appl. Catal. A 505 (2015) 417–421.
[50] E. Pedrajas, I. Sorribes, K. Junge, M. Beller, R. Llusar, ChemCatChem 7 (2015) 2675–2681.
[51] S.S. Chou, B. Kaehr, J. Kim, B.M. Foley, M. De, P.E. Hopkins, J. Huang, C.J. Brinker, V.P. Dravid, Angew. Chem. Int. Ed. 52 (2013) 4160–4164.
[52] J. Kibsgaard, Z. Chen, B.N. Reinecke, T.F. Jaramillo, Nature Mater. 11 (2012) 963–969.
[53] Y. Sun, X. Hu, W. Luo, Y. Huang, ACS Nano 5 (2011) 7100–7107.
[54] The reduction of MoO_x by N_2H_4 to Mo(0) and the oxidation of Mo(0) by nitrobenzene to aniline.
[55] S.K. Singh, Q. Xu, J. Am. Chem. Soc. 131 (2009) 18032–18033.
[56] S.K. Singh, X.B. Zhang, Q. Xu, J. Am. Chem. Soc. 131 (2009) 9894–9895.
[57] X. Chen, T. Zhang, P. Ying, M. Zheng, W. Wu, L. Xia, T. Li, X. Wang, C. Li, Chem. Commun. (2002) 288–289.
[58] L. He, Y. Huang, A. Wang, X. Wang, X. Chen, J.J. Delgado, T. Zhang, Angew. Chem. Int. Ed. 51 (2012) 6191–6194.
[59] F. Haber, Z. Elektrochem. Angew. Phys. Chem. 22 (1898) 506–514.
[60] Y. Mikami, A. Noujima, T. Mitsudome, T. Mizugaki, K. Jitsukawa, K. Kaneda, Chem. Lett. 39 (2010) 223–225.
[61] K. Shimizu, Y. Miyamoto, A. Satsuma, J. Catal. 270 (2010) 86–94.
[62] S.K. Singh, A.K. Singh, K. Aranishi, Q. Xu, J. Am. Chem. Soc. 133 (2011) 19638–19641.
[63] A. Furst, R.C. Berlo, S. Hooton, Chem. Rev. 65 (1965) 51–68.
[64] X.N. Guo, C.H. Hao, G.Q. Jin, H.Y. Zhu, X.Y. Guo, Angew. Chem. Int. Ed. 53 (2014) 1973–1977.
[65] L. Hu, X.Q. Cao, L. Chen, J.W. Zheng, J.M. Lu, X.H. Sun, H.W. Gu, Chem. Commun. 48 (2012) 3445–3447.
[66] H. Zhu, X. Ke, X. Yang, S. Sarina, H. Liu, Angew. Chem. Int. Ed. 49 (2010) 9657–9661.
[67] X. Chen, T. Zhang, M. Zheng, Z. Wu, W. Wu, C. Li, J. Catal. 224 (2004) 473–478.
[68] J.P. Contour, G. Pannetie, J. Catal. 24 (1972) 434–445.
[69] J. Block, G. Schulz-Ekloff, J. Catal. 30 (1973) 327–329.
[70] M. Daage, R.R. Chianelli, J. Catal. 149 (1994) 414–427.
[71] T.F. Jaramillo, K.P. Jorgensen, J. Bonde, J.H. Nielsen, S. Horch, I. Chorkendorff, Science 317 (2007) 100–102.
[72] J.V. Lauritsen, J. Kibsgaard, S. Helveg, H. Topsoe, B.S. Clausen, E. Laegsgaard, F. Besenbacher, Nat. Nanotechnol. 2 (2007) 53–58.
[73] A. Albu-Yaron, M. Levy, R. Tenne, R. Popovitz-Biro, M. Weidenbach, M. Bar-Sadan, L. Houben, A.N. Enyashin, G. Seifert, D. Feuermann, E.A. Katz, J.M. Gordon, Angew. Chem. Int. Ed. 50 (2011) 1810–1814.
[74] H.I. Karunadasa, E. Montalvo, Y.J. Sun, M. Majda, J.R. Long, C.J. Chang, Science 335 (2012) 698–702.
[75] D.S. Kong, H.T. Wang, J.J. Cha, M. Pasta, K.J. Koski, J. Yao, Y. Cui, Nano Lett. 13 (2013) 1341–1347.
[76] M. Asadi, B. Kumar, A. Behranginia, B.A. Rosen, A. Baskin, N. Repnin, D. Pisasale, P. Phillips, W. Zhu, R. Haasch, R.F. Klie, P. Kral, J. Abiade, A. Salehi-Khojin, Nat. Commun. 5 (2014) 4470.
[77] I.N. Yakovkin, N.V. Petrova, Chem. Phys. 434 (2014) 20–24.
[78] C. Tsai, K. Chan, J.K. Norskov, F. Abild-Pedersen, Surf. Sci. 640 (2015) 133–140.